Functional biomimetic design of 3D printed polyether-ether-ketone flexible chest wall reconstruction implants for restoration of the respiration

Changning Sun [a,b,c,1], Enchun Dong [a,b,1], Yucong Tian [a,b], Jianfeng Kang [d], Jibao Zheng [a,b], Qing Zhang [a,e], Lei Wang [f], Chaozong Liu [c], Ling Wang [a,b,*], Dichen Li [a,b,*]

[a] State Key Laboratory for Manufacturing System Engineering, School of Mechanical Engineering, Xi'an Jiaotong University, 710054 Xi'an, ShaanXi, China
[b] National Medical Products Administration (NMPA) Key Laboratory for Research and Evaluation of Additive Manufacturing Medical Devices, Xi'an Jiaotong University, 710054 Xi'an, ShaanXi, China
[c] Institute of Orthopaedic & Musculoskeletal Science, University College London, Royal National Orthopaedic Hospital, Stanmore HA7 4LP, UK
[d] School of Mechatronic Engineering and Automation, Foshan University, 528225 Foshan, Guangdong, China
[e] Centre for Medical Device Evaluation, National Medical Products Administration (NMPA), 100081 Beijing, China
[f] Departments of Thoracic Surgery, Tangdu Hospital, Airforce Medical University, 710038 Xi'an, ShaanXi, China

ARTICLE INFO

ABSTRACT

The lack of deformability of rigid chest wall reconstruction (CWR) implants presents a challenge in reducing postoperative respiratory function in patients with large chest wall defects. Flexible poly-ether-ether-ketone (PEEK) CWR implants, consisting of rib components with elliptical cross-section and costal cartilage components featuring wavy structures, were developed with adjustable design parameters that allow quantitative restoration of respiratory function. During the design process, the equivalent elastic moduli of the rib and costal cartilage components were parametrically adjusted in a validated finite element (FE) model of the chest wall to maximise chest wall deformation during respiration, while considering mechanical safety as the boundary condition. The optimal equivalent elastic moduli were then translated into design parameters for the rib and costal cartilage components, based on a database relating the equivalent elastic modulus to the design parameters of the components with elliptical cross-section and wavy structures. The flexible PEEK CWR implant increased the difference in chest circumference during respiration by 12.2% compared to rigid PEEK implant in a clinical case-based study. This study presents a strategy to address the reduced respiratory function in 3D printed CWR implants, providing a pathway for quantitative restoration of respiratory function through parameterised optimisation.

1. Introduction

Chest wall defects resulting from chest wall tumours, trauma, congenital malformation, or massive infection, are generally considered to be reconstructed with artificial implants if they exceed an area of 5 cm × 5 cm [1,2]. Bony chest wall reconstruction (CWR) using rigid materials plays an important role in restoring of thoracic integrity, stability and respiratory function [3].

Due to the marked differences in anatomical morphology and the specific characteristics of the chest wall defects in individual patients, customised implants fabricated by additive manufacturing (AM) technology, commonly known as 3D printing, were believed to be a promising approach to reconstruct large chest wall defects. Both titanium alloy and polyether-ether-ketone (PEEK) have been employed in published clinical studies. In 2014, Turna et al. [4] reported the first clinical application of 3D printed customised titanium implants for bony CWR using 3D printing technology. Since then, several multidisciplinary teams of surgeons and engineers around the world have published the clinical trials involving rib and sternal implants made by similar technology [5–10]. The first clinical application of PEEK material in bony CWR was reported by Kang et al. [11], and Wang et al. [12] reviewed their series cases of CWR surgeries using 3D printed PEEK customised implant dating back to 2017. One of the most distinct benefits of 3D printed CWR implants was the excellent short-term cosmetic results,

---

* Corresponding authors at: State Key Laboratory for Manufacturing System Engineering, School of Mechanical Engineering, Xi'an Jiaotong University, China.
 E-mail addresses: menlwang@mail.xjtu.edu.cn (L. Wang), dcli@mail.xjtu.edu.cn (D. Li).
 [1] These authors contributed equally to this manuscript.

which help to preserve the thoracic morphology [5,13,14]. Additionally, the incorporation of digital surgical planning along with 3D printed customised implants has been found to reduce operating time and intraoperative blood loss. However, patients complained of reduced respiration or breathing pain after implantations, and clinical follow-ups also confirmed a 12 %–16 % reduction in forced vital capacity (FVC) post-operatively for patients with PEEK implants [12,15]. Although there is no direct clinical evidence, it is presumed that the reduction in FVC for 3D printed titanium CWR implants would be even greater than that of PEEK implants due to the significantly higher elastic modulus of titanium alloy. In the natural chest wall, the elongation and deformation of the costal cartilage during inspiration contributes to changes in thoracic dimension. But CWR implants made of rigid materials such as PEEK or titanium alloy have a much lower deformability than that of costal cartilage, thus failing to provide sufficient expansion of the thorax during respiration.

To solve the challenge of respiratory function in rigid CWR implants, a strategy based on spring-like structure was developed to obtain flexible implants. Aragón et al. [16] designed a specific structure with bending capabilities to simulate natural chondrosternal articulations, and reported that rib implants with this specific structure at the costal cartilage section, fabricated by 3D printed titanium alloy, reduced the FVC by 12 %. Moradiellos et al. [17] developed titanium rib implants with a "Greek wave" folding pattern, acting as a functional spring capable of extension or compression during respiratory cycles [18]. Although the CWR implants with "Greek wave" design was applied in the clinic, but post-operative follow-up data on respiratory function have not been published. The spring-like structure made of titanium alloy reduced the stiffness of the CWR implants, but the high elastic modulus of titanium alloy (typically 100–120 GPa [19,20]) still resulted in a stiffness of the spring-like structure much higher than that of natural costal cartilage (8.7–12.6 MPa [21]). The strategy of a spring-like structure was also implemented in PEEK CWR implants. In previous studies by Zhang et al. [22] and Kang et al. [23], a method was developed to mimic the mechanical properties of costal cartilage through a wavy elastic structure made from PEEK material. The equivalent elastic modulus of mimicked costal cartilage, fabricated by materials extrusion technology [24–26], was adjusted to a range (0.5–17.3 MPa [22]) similar to that of natural costal cartilage, while meeting the strength requirements for chest compression. Animal studies demonstrated that the key indicators related to respiration, such as chest circumference, pulmonary ventilation volume, and dynamic compliance, were restored to healthy values 7 months after the implantation of PEEK CWR implants with the wavy elastic structure [23]. Till now, the flexible PEEK CWR implants developed by Zhang et al. [22] and Kang et al. [23] have not been used in the clinic.

The mechanical principle behind the 3D printed flexible CWR implants to optimise respiratory function was to mimic the mechanical properties of costal cartilage by designing elastic structures, thereby restoring the expanding and contracting ability of the reconstructed chest wall during respiration. Despite some specific successes, achieving a healthy level of respiratory function in the clinical application of 3D printed flexible CWR implants remains a challenge. This challenge is magnified by the variability in respiratory function and chest wall defects among individuals. Each patient has unique requirements for the expansion and contraction behaviour of CWR implants during respiration, leading to different demands on the mechanical performance of CWR implants under respiratory loads. Precise structural design is therefore essential to quantitatively restore the respiratory capacity of the individual patient with the CWR implant. To the best of the author's knowledge, this is the first investigation in 3D printing CWR implants that considers the quantitative restoration of a specific patient's respiratory function through structural design.

Given the challenge of designing flexible CWR implants that align with the respiratory function of individual patients, this study develops a strategy for customising flexible CWR implants consisting of rib and costal cartilage components. Firstly, the mechanical properties of the rib and costal cartilage components of the CWR implants are investigated through mechanical experiments to understand the influence of structural parameters. Secondly, the quantitative effect of the mechanical properties of the rib component and costal cartilage components on the expansion and contraction of the reconstructed thoracic cage under respiratory loads is simulated by finite element (FE) models. Finally, a clinic-based demonstration shows how to restore respiratory function to a healthy level through the structural design of flexible PEEK CWR implants. This study provides a feasible design methodology for customised flexible PEEK CWR implants with the objective of restoring respiratory function.

## 2. Materials and methods

2.1. FE model of the natural thorax

An accurate FE model capable of predicting the deformation of the chest wall during respiration serves as the foundation for studying the effect of the design of flexible CWR implants on the respiratory function. In this study, an FE model of the natural thorax was established and validated by comparing the simulated results with current research.

The 3D model of the natural thorax (Fig. 1A), including the sternum, ribs, and costal cartilage, was reconstructed based on computed tomography (CT) data from a healthy adult male volunteer of medium stature with normal thoracic morphology and function. The reconstruction process was performed using Mimics 21.0 (Materialise, Belgium) and Geomagic Studio 12.0 (Geomagic, USA) software. The surrounding muscles, including the diaphragm, sternocleidomastoid (SCM), levatores costarum breves (LCB), external intercostal muscles (EIM), internal intercostal muscles (IIM), abdominal internal oblique (AIO), abdominal external oblique (AEO), and rectus abdominis (RA), were added to simulate the respiratory function. The diaphragm, which is one of the most important respiratory muscles, accounting for 60–80 % of the inspiratory function [27], was constructed in SolidWorks 2016 software (Dassault, France) based on the anatomical morphology and dimensions measured in the CT images. It consisted of the central tendon, muscle belly and muscle fibre (Fig. 1B). The remaining muscles, such as EIM and AEO, were built using line segments in Hypermesh 12.0 software (Altair, USA) based on the anatomical characteristics of the thorax.

The 3D model of the thorax was meshed using HyperMesh 12.0, and LS-PrePost V 4.3.38 software (ANSYS, USA) was used for pre-processing of the FE model. The sternum, ribs, and costal cartilage were meshed using the four-node tetrahedron linear element (C3D4). The diaphragm was meshed using the four-node quadrilateral element (S4R). The remaining muscles were meshed using the truss element (T3D2). Mesh sensitivity was checked and an element size of 1 mm was selected. To simulate the rotation of the costovertebral joint and the costotransverse joint (Fig. 2A.1), the joint-revolute unit was used, considering the physiological characteristics of the human body. The cartilage was bounded to the sternum and ribs to simulate amphiarthroses (Fig. 2A.2). The ends of the muscle fibres were coupled to the ribs to drive the thoracic movement during respiration. The distal ends of the SCM, AIO, AEO and RA were fixed. The interface between the diaphragm and the thorax was set as frictionless contact to simulate sliding during respiration (Fig. 2A.3).

The material properties of the sternum, ribs, costal cartilage, and the diaphragm are shown in Table 1. The Hill skeletal muscle model was employed to simulate the muscle fibres. The basic Hill model consists of passive parallel elastic units (PE) and active contractile units (CE). The total muscle stress can be obtained by summing the stress vectors from both units, as shown in equation (1):

$$\sigma = \sigma_{PE} + \sigma_{CE} \tag{1}$$
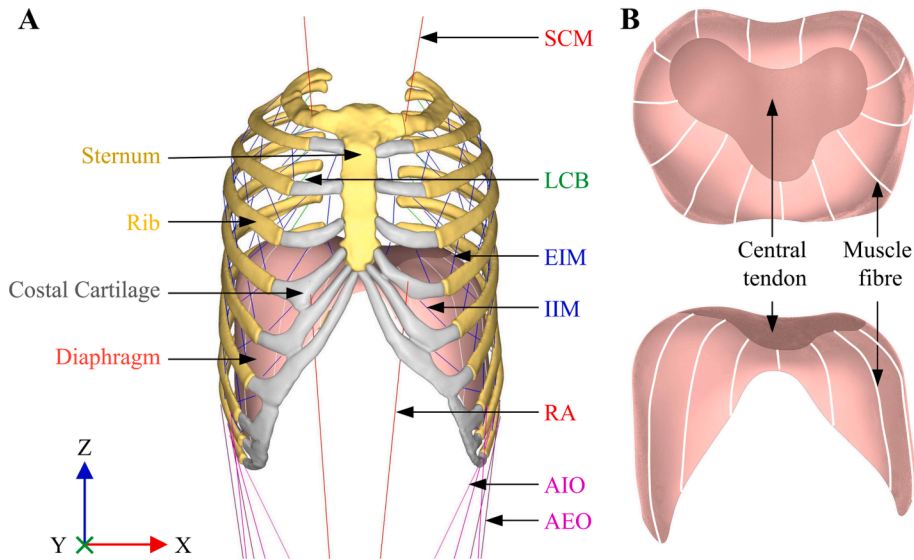
Fig. 1. 3D model of the natural thorax. (A) Bones, cartilage, muscles and diaphragm. (B) The model of the diaphragm. (SCM: sternocleidomastoid; LCB: levatores costarum breves; EIM: external intercostal muscles; IIM: internal intercostal muscles; AIO: abdominal internal oblique; AEO: abdominal external oblique; RA: rectus abdominis).
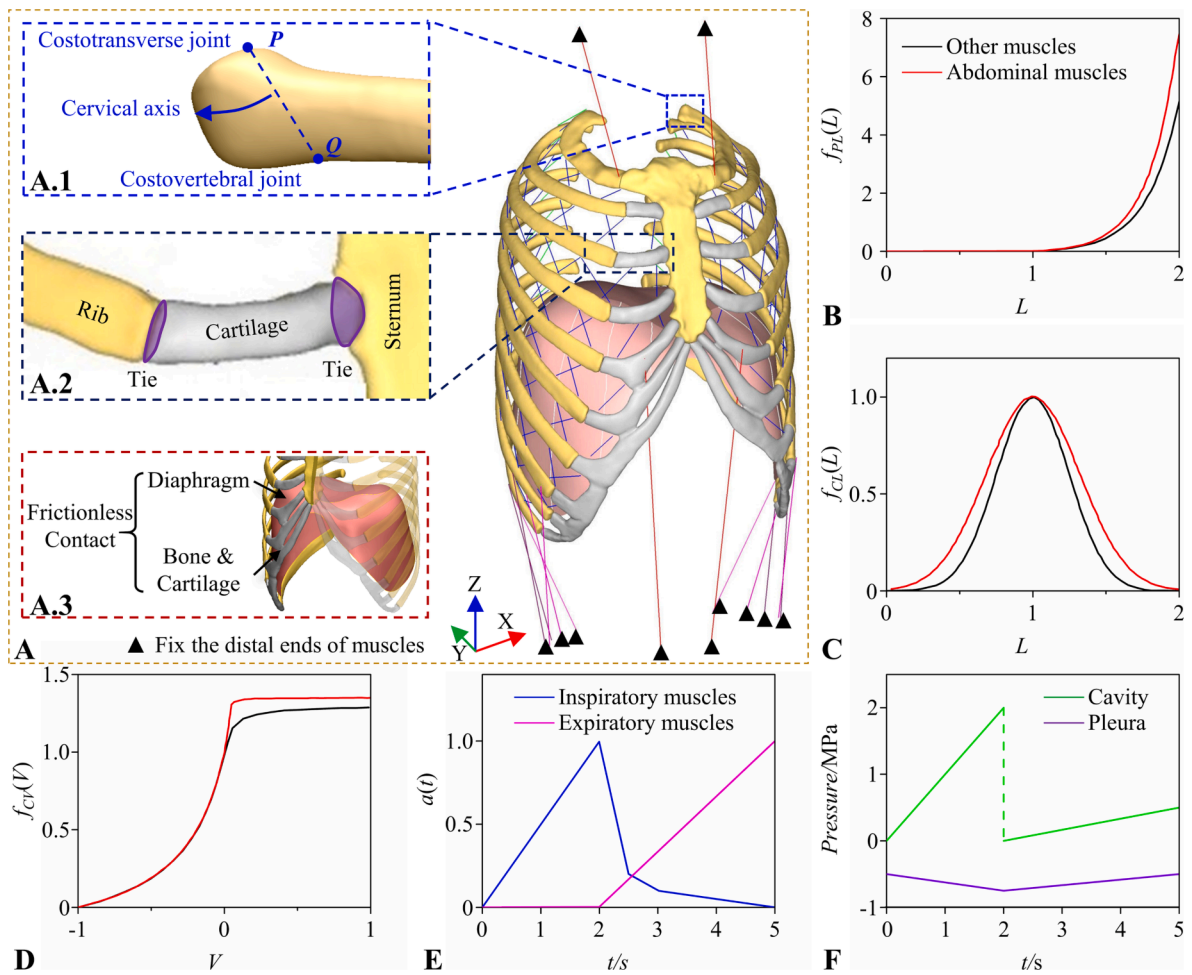
Fig. 2. Finite element model setup of the natural thorax. (A) Boundary conditions, contacts and interactions of the thorax FE model. (A.1) The boundary conditions of the connection between ribs and vertebrae. (A.2) The constraint among ribs, costal cartilage and sternum. (A.3) The contact between diaphragm and chest wall. The relationships between (B) passive muscle stress and the relative length of muscles fibres, (C) active muscle stress and the relative length of muscles fibres, (D) active muscle stress and relative contractive speed. (E) The activation level of muscles in respiration cycle. (F) The pressure of cavity and pleura in respiration cycle. In (E) and (F), time before 2 s is the inspiration stage, after 2 s is the expiration stage.

Table 1
Mechanical properties of components in FE model.

Component	Density /kg/mm^3	Elastic modulus/GPa	Yield strength /MPa	Poisson's ratio	Ref.
Sternum	1.5×10^{-6}	11.5	90	0.3	[30–32]
rib	1.5×10^{-6}	5	88	0.3	
Costal cartilage	1.5×10^{-6}	0.05	7	0.4	[32–34]
Muscle of diaphragm	1.3×10^{-6}	0.053	—	0.33	[35–37]
Tendon of diaphragm	1.3×10^{-6}	0.033	—	0.33	
PEEK	1.32×10^{-6}	2.9	90	0.3	[38]

where σ denotes the muscle stress; σ_{PE} denotes the stress of the PE; σ_{CE} denotes the stress of the CE. σ_{PE} was described by Eq. (2):

$$\sigma_{PE} = \sigma_{\max} f_{PL}(L) \tag{2}$$

where σ_{max} denotes maximum isometric shrinkage stress.

According to the previous studies, the σ_{max} of LCB, EIM and IIM was 0.4 MPa [28], the σ_{max} of SCM, AIO, AEO and RA was 0.46 MPa [29], the σ_{max} of diaphragm fibres was 0.26 MPa [28]. $f_{PL}(L)$ was the passive stress-relative length relation, as shown in Fig. 2B. σ_{CE} was a function of muscle length, speed, and activation, as shown in Eq. (3):

$$\sigma_{CE} = \sigma_{\max} a(t) f_{CL}(L) f_{CV}(V) \tag{3}$$

where $a(t)$ denotes the muscle state ("0" for restrain and "1" for active); $f_{CL}(L)$ denotes the active stress-relative length relation, as shown in Fig. 2C; $f_{CV}(V)$ denotes the active stress-relative shrinkage velocity relation, as shown in Fig. 2D.

Two loading conditions were applied to the FE model to simulate chest compression during cardiopulmonary resuscitation (CPR) and spontaneous respiration. For the chest compression simulation, a displacement of 50 mm towards the + Y direction was applied to an area approximately the size of a palm at the distal sternum, with a duration of 0.6 s to mimic CPR. For the spontaneous respiration, the respiratory muscles were activated to follow the respiratory cycle shown in Fig. 2E. Abdominal pressure and pleural pressure [39] (Fig. 2F) were respectively applied to the lower surface of the diaphragm and the inner surface of the thoracic cavity, respectively, to simulate natural respiratory motion. The FE analysis was performed using the LS-DYNA R11.0 solver software (ANSYS, USA).

2.2. Characterisation of the equivalent mechanical properties of rib and costal cartilage components

The flexible CWR implant was divided into a rib component and a cartilage component, as shown in Fig. 3B, referring to the anatomical structures of human rib and costal cartilage. The demarcation between the rib and costal cartilage components of the CWR implant followed the natural anatomical structure. Expanding on the variable cross-section design method along the centroid trajectory of rib established by Kang et al. [11], a simplified design method for the rib component with a fixed cross-section was developed. The cross-section of the rib component was designed as a hollow ellipse, as presented in Fig. 3A, with a solid outer

Table 2
Design parameters of the flexible rib and costal cartilage implant.

Implant	Parameter	Value			
Rib	Length of long axis a/mm	5	6	7	8
	Length of short axis b/mm	3	4	5	/
	Wall thickness t/mm	1	2	3	/
	Rotation angle θ/°	0	45	60	90
	Filling rate r/%	10	50	100	/
Costal cartilage	Amplitude h/mm	4	5	6	7
	Thickness d/mm	4	6	8	10
	Wavelength λ/mm	6	7	8	9
	Line width w/mm	1.5	2	/	/
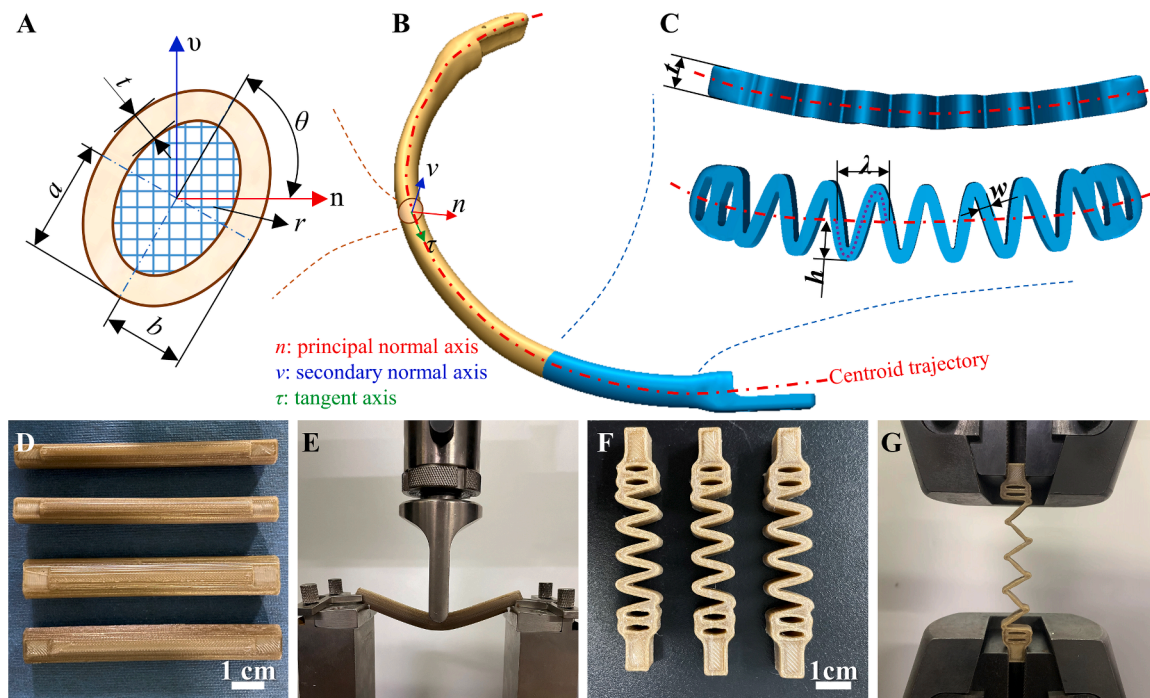
Fig. 3. The design and mechanical tests of 3D printed flexible PEEK rib implants and costal cartilage implants. (A) Design of the rib implants. (B) A schematic diagram of a typical rib/costal cartilage integrated implant. (C) Design of the costal cartilage implants with a wavy structure. Three-point bending samples (D) and testing (E) of the rib implants. Tensile samples (F) and testing (G) of the costal cartilage implants.

wall and internally filled with a porous structure. Table 2 shows the five design parameters that characterise the elliptical cross-section. Among these parameters, it should be noted that θ represents the angle between the long axis of the ellipse and the principal normal axis (n) of the centroid trajectory of the natural rib. The inclusion of θ as one of the design parameters was justified by the fact that, on one hand, the angle between the ellipse fitted to the cross-section at different locations of the natural rib and the principal normal of the trajectory varies. On the other hand, the bending performance of the elliptical cross-section is also influenced by θ. The costal cartilage component was designed as an elastic wavy structure with four design parameters, as shown in Fig. 3C and Table 2. The centreline trajectory of the wavy structure also mirrored that of natural costal cartilage.

Mechanical tests were employed to investigate the effect of design parameters on the mechanical properties of the rib and costal cartilage components. Following the principles of orthogonal testing, the mechanical tests for the rib and costal cartilage components were set as 16 experimental groups as detailed in Table S1 and Table S2 in Supplementary File 1, respectively. For the rib components, all specimens have a length of 100 mm. As for the costal cartilage components, the specimen lengths vary with the cycle, and the length of each set of specimens is recorded in Table S2 in Supplementary File 1. The PEEK (450 PF, Victrex, UK) samples were fabricated using Fused filament fabrication technology (Surgeon Plus, Jugao AM, China) with the following process parameters: nozzle temperature of 420 °C, printing speed of 50 mm/s, bead width of 0.4 mm, layer thickness of 0.2 mm, bed temperature of 25 °C and raster angle of ± 45 °C. The mechanical properties of the rib and costal cartilage components were measured using a universal mechanical testing machine (SANS CMT4304, MTS, America). During respiration or chest compressions, the volume change of the thorax is mainly achieved through bending deformation of the ribs and tensile deformation of the costal cartilage. Therefore, three-point bending tests were performed to determine the bending elastic modulus and strength of the rib component. The tests were performed with a span of 80 mm and a loading speed of 2 mm/min. Uniaxial tensile tests were carried out to assess the costal cartilage component at loading speed of 2 mm/min. The experimental temperature and humidity were 25 ～ 28 °C and 40 ～ 60 %, respectively. Each group consisted of six specimens.

Following to the procedure described in Supplementary File 2, the equivalent elastic moduli of the rib and costal cartilage component were calculated from the force–displacement curves measured in three-point bending tests and uniaxial tensile tests, respectively. Parameters that significantly affected the mechanical properties were identified by variance analysis. This led to the establishment of two databases: one for the rib component with a hollow elliptical cross-section, and another for the costal cartilage component with a wavy structure. Both databases provided the relationship between the equivalent elastic modulus and design parameters.

2.3. Parameterized study of the elastic modulus of rib and costal cartilage components

In this study, a parametric method was developed based on the equivalent mechanical properties of the rib and costal cartilage components to achieve optimal restoration of respiration postoperatively. First, an equivalent FE model of the CWR implant and the natural thorax was established. Building upon the FE model of the natural thorax in section 2.1, an in-suit designed CWR implant involving only the 5th rib, was divided into rib component, costal cartilage component, and connecting component. The interfaces between the connecting component and the residual bone were tied to simulate the immediate fixation in surgery such as screws or wires. The EIM surrounding the CWR implant was converted to a deactivated statue to simulate the passive force, which restricts the movement of the CWR implant without active traction after the resection of the EIM. The remaining boundary conditions, loads, mesh sizes, element types, and material properties were consistent with the natural thorax model described in Section 2.1.

In the equivalent CWR implant-natural thorax FE model, the influence of the equivalent bending elastic moduli of the rib component (E_r) and the equivalent tensile elastic modulus of the costal cartilage component (E_c) on the deformation of the thorax during respiration was investigated. The aim was to determine the optimal equivalent elastic modulus for both components that would maximise the benefit to respiratory function. For the FE analysis, four different values were assigned to both E_r and E_c, resulting in 16 groups of FE analysis, as detailed in Table S3 in Supplementary File 1. The indications for evaluating restoration of respiration in the FE analysis including the length variation of the chest wall in the medial–lateral and anterior-posterior axes during a respiratory process on the cross-section of human, denoted as Δx and Δy, respectively, and the difference in chest circumference were represented as ΔC.

To validate the equivalent CWR implant-natural thorax FE model, realistic models of the CWR implant, with a cross-section of hollow ellipse for the rib component and a wavy structure for the costal cartilage component, were developed to predict the deformation of the chest wall during respiration. Only two realistic models with minimum and maximum elastic modulus were employed for validation. The same indications used to evaluate the deformation of the thorax in the equivalent CWR implant-natural thorax FE model were employed for comparison with the realistic models. In the realistic models, those indications were denoted as $\Delta x'$, $\Delta y'$ and $\Delta C'$. Furthermore, the stress obtained from the realistic models served to assess the safety of the CWR implant.

2.4. Design of CWR implants based on a clinical case

Fig. 4 illustrates the framework to design the flexible CWR implants in clinical applications. First, a 3D model of the defected chest wall with tumour was reconstructed from CT data. Second, the implant geometry, including the rib and costal components, was in-suit designed based on the surgical plan. Third, the elastic modulus of the rib and costal cartilage components were varied to simulate the difference in chest circumference (ΔC) and compared with the expected difference in chest circumference (ΔCE). The ΔCE was determined by the clinicians based on the expected post-operative respiratory function of the patient. Parametric studies of the equivalent elastic modulus of the rib (E_r) and costal cartilage (E_c) components were conducted with the aim of minimising the discrepancy between ΔC and ΔCE. Fourth, the optimised values of E_r and E_c were traversed into the design parameters of the rib and costal cartilage components based on the databases established in section 2.2. Fifth, the stress of the optimised flexible CWR implant during chest compression was calculated by FE analysis to check the mechanical safety of the implant. Finally, a 3D model suitable for 3D printing was generated, typically in STL format.

To illustrate the design framework, a case study was conducted based on a previously reported PEEK rib implant [11]. Three combinations of E_r and E_c that met respiratory demands were chosen, along with the rigid implant as a reference. FE analysis was employed to compare the respiratory restoration and the mechanical safety of the implant with different design parameters.

3. Results

3.1. FE analysis of the natural thorax

The results of the deformation of the natural chest wall under a chest compression of 5 mm are shown in Fig. 5A and 5B. Fig. 5A presents the deformation pattern of the natural chest wall, displaying a V-shaped pattern. The reaction force corresponding to the compression displacement is illustrated in Fig. 5B and compared with the data obtained from the "typical man" model established by Gruben et al. [40], demonstrating good consistency.
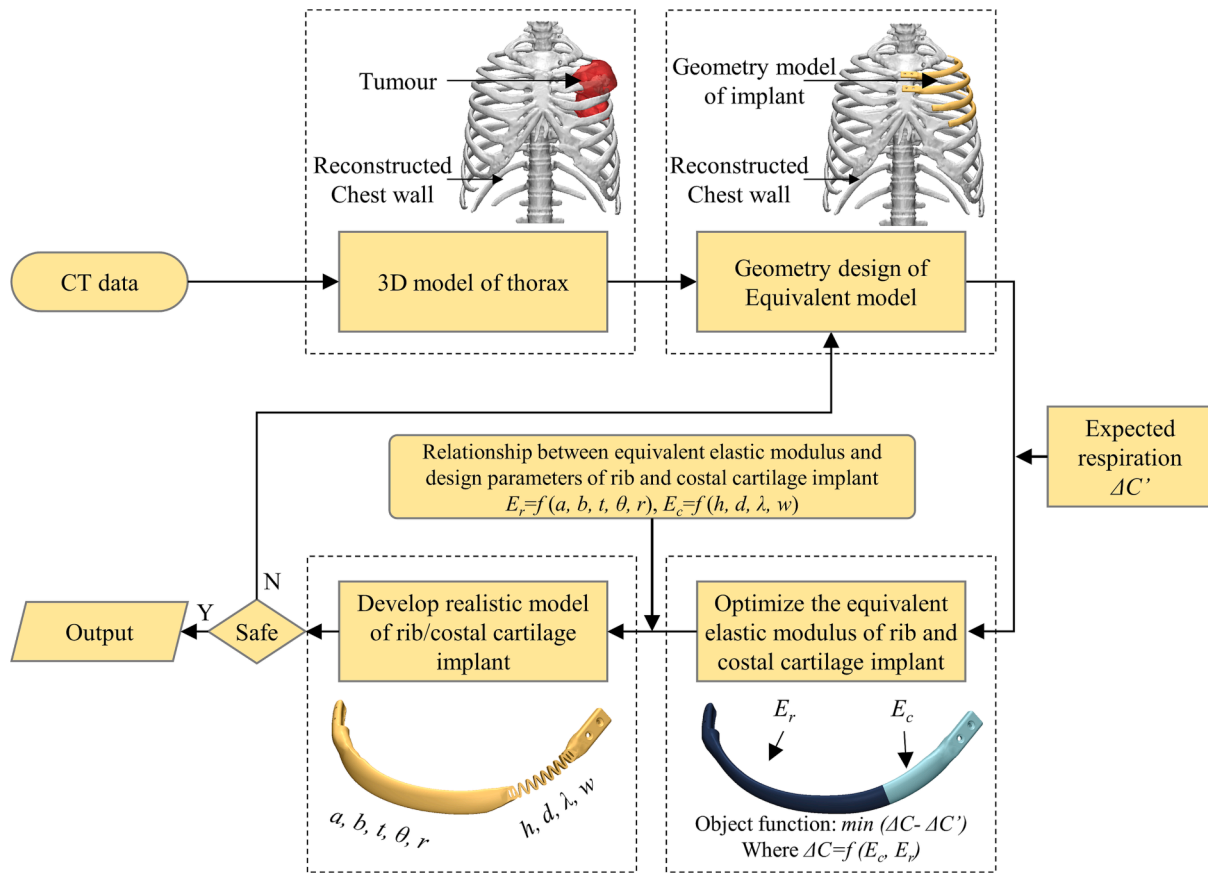
Fig. 4. Design framework for the flexible rib/costal cartilage CWR implants aiming to restore respiration function.

The deformation distribution of the natural thorax in the sagittal and coronal planes during respiration is illustrated in Fig. 5C and 5D, respectively. At the end of the inspiration phase, occurring in the 2 s of a respiratory cycle, the anterior-posterior distance of the chest wall, measured on the cross-section near the fourth rib, increased by 7.77 mm, while the medial–lateral distance increased by 8.49 mm. During the expiratory phase, which occurs between 2 and 5 s of the respiration cycle, the anterior-posterior distance of the chest wall was decreased of 12.13 mm, and the medial–lateral distance decreased by 6.83 mm. The difference in chest circumference between the end of inspiration and expiration amounted to 61 mm.

Fig. 5E and F illustrate the pump handle angle and the bucket handle angle of each rib at the end of inspiration and expiration, respectively. The angles obtained from the experiments and simulations conducted by Wilson et al. [41] and Zhang et al. [42] are also shown to validate the natural thorax FE model in this study.

3.2. Mechanical properties of the rib and costal cartilage components

The stiffness, bending strength and equivalent bending elastic modulus of rib components with different design parameters were detailed in Table S1, Supplementary File 1. It was determined that only the length of long axis (a) and short axis (b) of the ellipse have a significant influence on the equivalent bending elastic modulus by the variance analysis. The effect of both parameters on the equivalent elastic modulus of the rib component is illustrated in Fig. 6A. Detailed results concerning the mechanical properties of the wavy structure of the costal cartilage components can be found in Table S2, Supplementary File 1. The design parameters that had significant influence on the elastic modulus were amplitude (h) and line width (w), as shown in Fig. 6B. The equivalent bending elastic modulus of the rib component is adjustable

within a range of 0.35 GPa to 1.33 GPa, and the equivalent tensile elastic modulus of the rib cartilage components can be controlled within a range of 1.17 MPa to 65.88 MPa.

### 3.3. Design, validation and performance of equivalent CWR implant

The equivalent CWR implant is illustrated in Fig. 7A and B. The equivalent elastic moduli of the rib and costal cartilage components, which are shown in Fig. 7B, are evenly selected from four values within the range of equivalent elastic modulus obtained from mechanical experiments. Fig. 7C and D represent the geometry models and design parameters corresponding to the combinations of maximum and minimum elastic modulus of the rib and costal cartilage components, respectively. The distribution of von Mises stress for the flexible CWR implant with the maximum and minimum elastic moduli under the load of chest compression is shown in Fig. 7E and 7F, respectively. The highest stress of the CWR implants was found at the medial side of the wavy structure near the sternum. As presented in Fig. 7G, the relative errors between the predicted deformation of the chest wall in the cross-section by equivalent models and that by realistic models were less than 5 %, which provides evidence supporting the effectiveness of the equivalent models in predicting the thoracic deformation. Fig. 7H illustrates the impact of the equivalent elastic modulus of the rib and costal cartilage components on chest circumference during respiration, laying the foundation for designing flexible CWR implants for clinical cases.

3.4. Flexible CWR implant based on clinical case

Based on a published clinical case of PEEK rib implants [11], flexible CWR implants were design and compared to the rigid implant. As
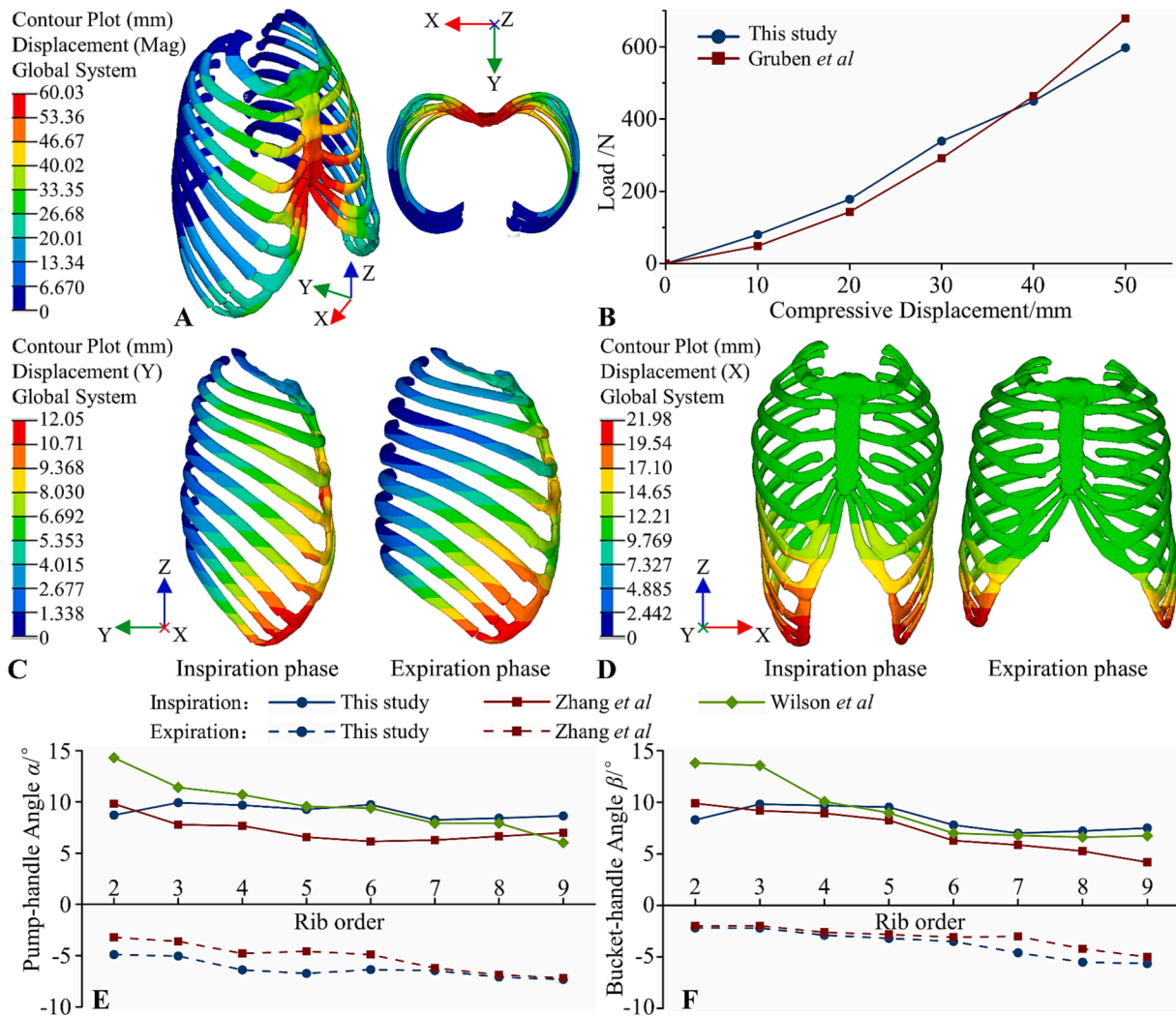
Fig. 5. The predicted deformations of natural thorax during chest compression and a respiratory process. (A) The deformation during chest compression. (B) The reaction load with the chest compressive displacement. (C) The deformation of natural thorax on sagittal view. (D) The deformation of natural thorax on coronal view. (E) The pump-handle angle of every ribs during a respiratory. (F) The bucket-handle angle of every ribs during a respiratory.
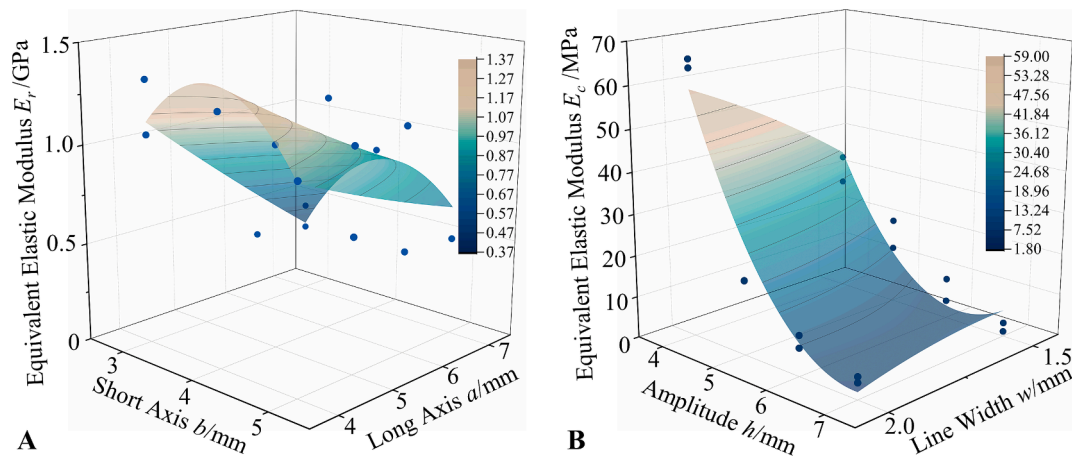
Fig. 6. The effect of design parameters on the (A) bending elastic modulus and (B) tensile elastic modulus of rib and costal cartilage, respectively.

presented in Fig. 8A, three flexible CWR implants, namely FA, FB and FC, were designed. To simplify the design process appropriately, an equivalent bending elastic modulus of 470 MPa was used for the rib component in all three CWR implants, which is a relative low value

within the range listed in Table S1, Supplementary File 1. The equivalent tensile elastic modulus of the costal cartilage components, along with their corresponding design parameters, are listed in Table 3. According to the quantitative relationship presented in Fig. 7H, which shows the
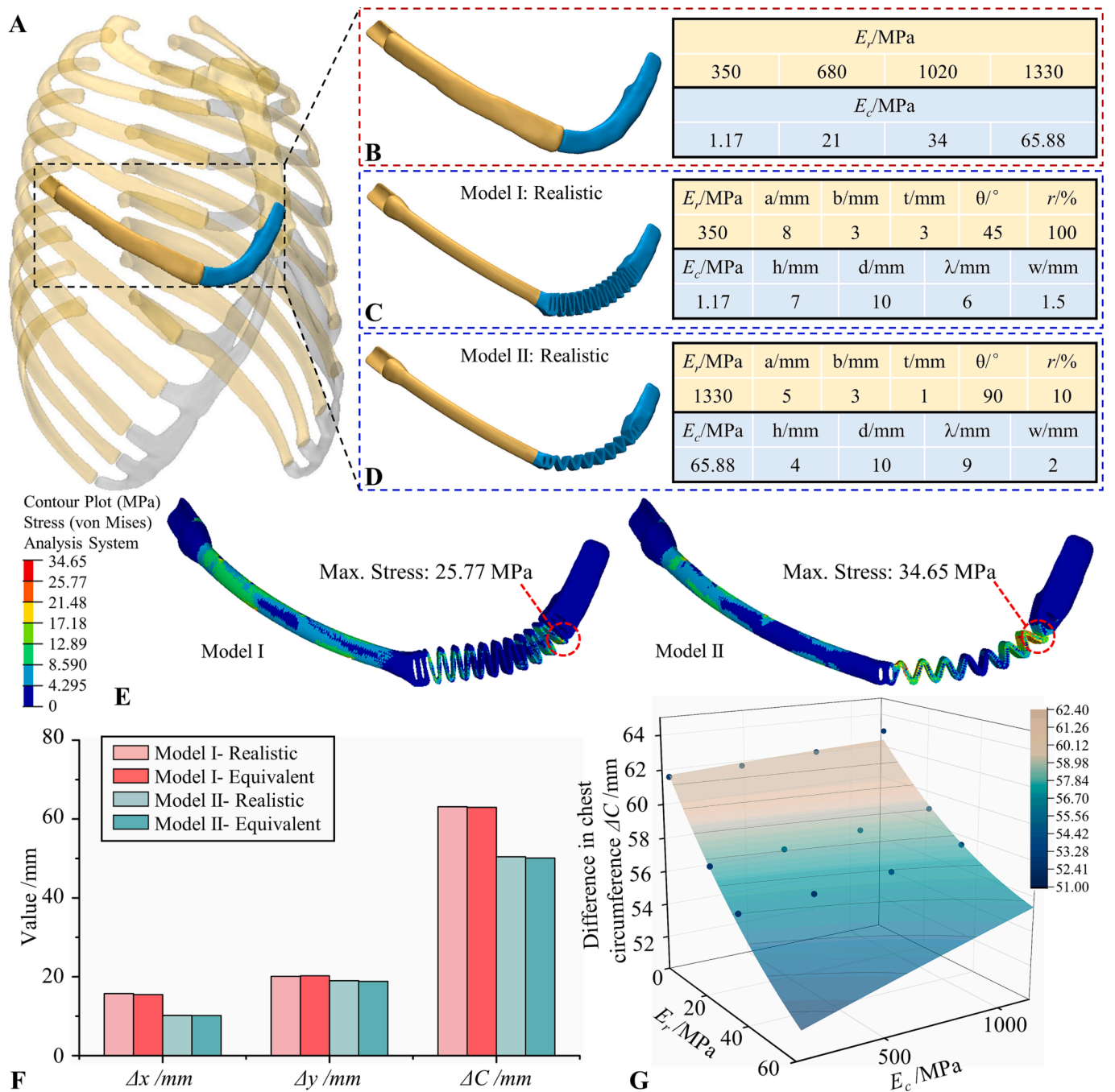
Fig. 7. The design and evaluation of equivalent CWR implant-natural thorax model. (A) The equivalent CWR implant model of 5th rib. (B) The values of E_r and E_c involved in the FE analysis. (C, D) The realistic CWR implant models. (E)The stress distribution of realistic CWR implant model I and model II on expiration phase. (F) The deformation of the natural thorax during a respiration on different direction. (G) Effect of the elastic modulus of rib and costal cartilage on the chest circumference.

effect of the equivalent modulus of rib and costal cartilage components on the differences in chest circumference during respiration, it is expected that the three flexible CWR implant, with design parameters listed in Table 3, would result in differences in chest circumference ranging from 57.7 to 59.7 mm. This range closely aligned with the actual differences in chest circumference observed during respiration of patients of similar age and the same gender. Comparing to the rigid implant, model FA exhibited a 12.2 % increase of the difference in chest circumference during respiration

The von Mises stress distribution of the implants and residual chest wall following the condition of chest compression is shown in Fig. 8B

and 8C, respectively. The results indicate that the rigid implant experienced the lowest peak stress, predicting 58.98 MPa at the connecting region with the sternum, whereas the chest wall experienced the largest stress compared to the flexible implants. Model FA, which had the lowest tensile modulus in the costal cartilage component, experienced the highest stress, reaching 89.64 MPa. Model FC exhibited the opposite pattern. It is worth mentioning that the yield strength of the 3D printed PEEK material, used as a benchmark, is around 90 MPa [43]. Fig. 8D, E and F illustrate the chest wall deformation on the cross-section during respiration along the medial–lateral axis and anterior-posterior axis, as well as the chest circumference. Overall, the implant FA exhibited
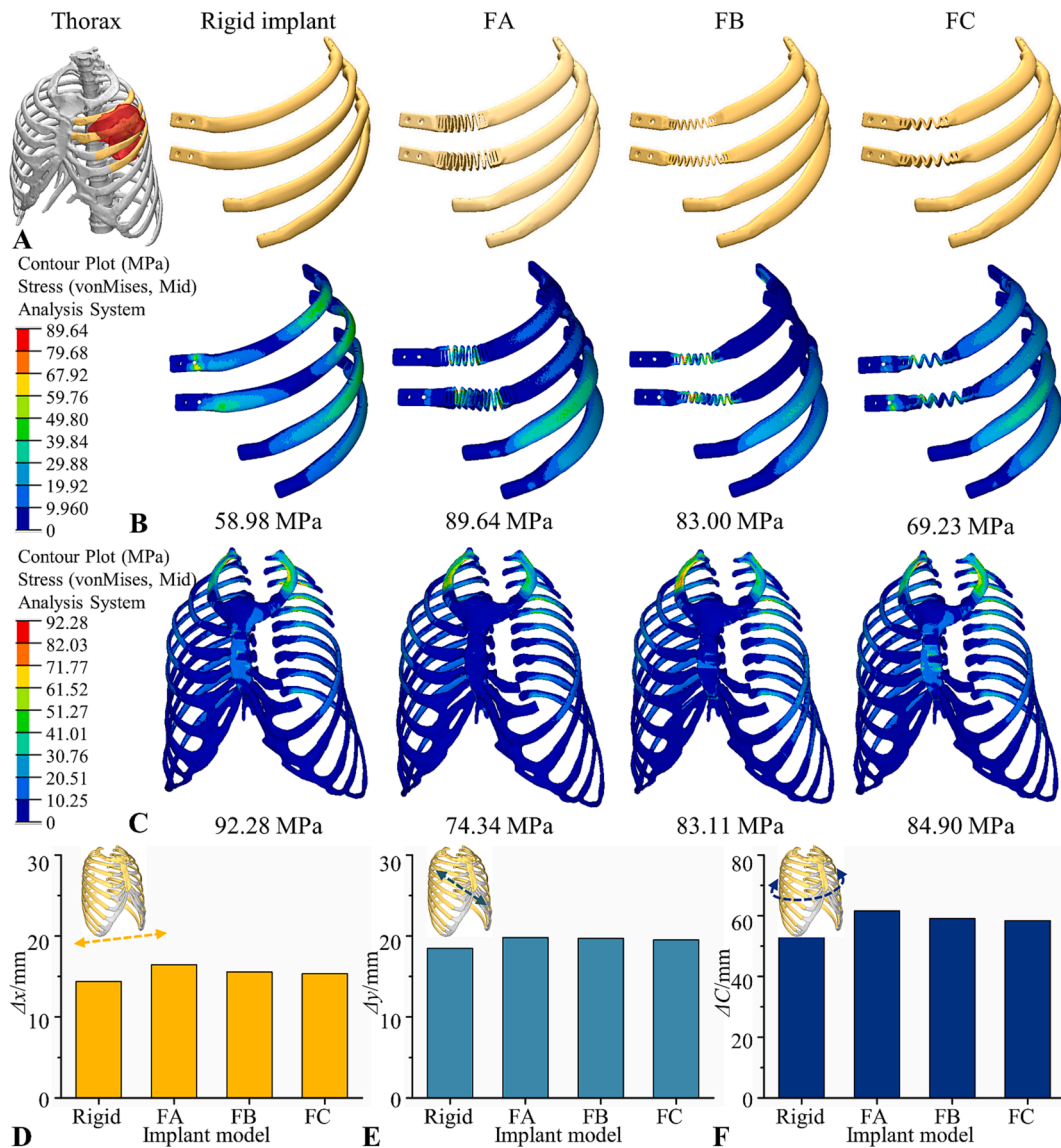
Fig. 8. Design and FEA results of flexible PEEK Rib/Costal Cartilage implants based on clinical case. (A) 3D model of rigid implant and flexible implants with different design parameters. The stress distribution of (B) implant and (C) residual thorax on chest compression. The deformation of the natural thorax during a respiration on (D) medial–lateral direction and (E) Anterior-posterior direction. (F) The difference in chest circumference during a respiration. (FA: Flexible model A; FB: Flexible model B; FC: Flexible model C).

Table 3
The design parameter of three typical rib implants based on clinical case.

Model name	Costal cartilage implant				
	h/mm	d/mm	λ/mm	w/°	E_c/MPa
FA	7	10	6	1.5	1.17
FB	4	4	6	1.5	34.2
FC	4	10	9	2	65.88

superior deformation capability during respiration. But the lower elastic modulus raised concerns about the mechanical safety of the costal cartilage components under the condition of external chest compression.

4. Discussion

Additive manufacturing offers a solution for repairing large chest wall defects. However, a complication of the damaged respiration postoperatively resulting from the reconstruction by rigid material, such as PEEK and titanium alloy remains to be solved. Based on previous studies [22,23], an in-situ parameterized design methodology based on equivalent mechanical properties was proposed to meet the requirements for implant deformation during respiration, which provide a practical approach to design the CWR implant. The methodology was demonstrated by a design process utilizing a real clinical case, and was found to improve the deformability of CWR implants during respiration while maintaining mechanical safety.

The design of CWR implants for quantitative restoration of respiration relies on accurate FE models predicting thoracic deformation during respiration. A comprehensive FE model of the natural thorax, including the ribs, costal cartilage, sternum, and the main respiratory muscle groups, was developed. Validation of the model confirmed its accuracy in two key aspects. Regrading external chest compression, the predicted deformation pattern of the natural thorax indicated a V-shaped chest depression similar to the actual situation [44], and the predicted reaction forces during compressive displacement on the sternum exhibited significant correlation with the experimental results of "typical man" acquired by Gruben et al. [40], particularly for displacements exceeding

than 2 cm. On the other side, the pump-handle and bucket-handle angles of each rib were employed to assess the accuracy of the FE model in predicting chest wall deformation during respiration. In inspiration, the pump-handle angle and bucket-handle angle of all ribs, except the second and ninth, were found to have a relative error of 10 % compare to the experimental results from Wilson et al. [41]. In expiration, both angles exhibited comparable trends to the simulated results of Zhang et al. [42], with a maximum deviation of 2°. During the respiration process, inspiration is primarily driven by the contraction of the diaphragm and EIM, causing the ribs to expand outward. Expiration is facilitated by the elastic recoil of the lungs and chest wall, with the RA contributing to the contraction of the chest wall by exerting a downward force on the ribs. Despite the omission of muscles, organs and their interaction of natural thoracic FE model, it was capable of predicting thoracic deformation based on the mechanism of respiratory motion by activating muscles and adjusting pleural and abdominal pressures. Thus, through comparison with published experimental and simulation studies, this investigation successfully validated the developed natural thoracic FE model.

The flexible CWR implant with integrated rib/costal cartilage designed in this study met clinical demands across three main criteria [45]. Firstly, to reconstruct the aesthetic appearance of the chest wall, the rib implant was customised based on the CT data of the specific patient. Although the geometric features of the natural chest wall were not fully replicated, the appearance of the defected chest wall was restored by extracting the central line of the ribs and creating a rib substitute with a constant cross-section using a parameter-controlled hollow ellipse. This approach can be defined as a "semi-customised" design. Secondly, the primary function of the CWR implant was to provide protection to the organs within the thoracic cavity. As chest compression represents one of the typical external loads experienced by the chest wall, the stress exerted on the flexible implant under such loading conditions was accurately predicted, providing an objective evaluation of the safety of CWR implants. Thirdly, the CWR implant was designed to exhibit deformation patterns and magnitudes comparable to those of the natural chest wall during respiration, thereby facilitating the restoration of the respiratory function postoperatively. The primary contribution of this study lies in the quantitative restoration of respiration through the flexible CWR implant, while simultaneously ensuring the restoration of the chest wall's appearance and the safety of the implant.

In order to design the structure of the flexible CWR implant efficiently, a novel methodology based on the equivalent model was presented in this study. The methodology was validated to evaluate its accuracy. When comparing the equivalent model with the realistic model of flexible PEEK CWR implant, the relative differences in the deformation of the chest wall in cross-section during respiration were all below 5 %. The consistency in thoracic deformation confirmed the effectiveness of the design methodology of the CWR implant based on the equivalent model. By adopting the equivalent model-oriented parametric design approach, instead of directly adjusting the design parameters of rib and costal cartilage components, the design process became more efficient and straightforward. Specifically, the procedure of parametric optimisation, which originally involved a total of nine parameters for the rib and costal cartilage components, was simplified to altering only two equivalent elastic moduli of them. The significant reduction in the number of design parameters not only decreased the complexity of the design process but also augmented the overall efficiency. In clinics, CWR implants are predominantly utilised for the reconstruction of extensive chest wall defects resulting from traumatic injuries or tumour-related conditions. Given the urgency often associated with these cases, the efficiency of the design process of the flexible CWR implant is also a critical factor, in addition to mechanical performance. The difference in chest circumference of postoperative CWR patients during respiration could be regulated within the range of 50.10 mm ~ 62.96 mm by adjusting the elastic modulus of the rib and costal

cartilage components. This controllable range effectively met the requirements of the majority of patients for the difference in chest circumference, which usually falls within the range of 40 mm to 70 mm.

The practicality of employing the flexible CWR implant design methodology in clinics was confirmed through a previously reported clinical case [11]. By manipulating the equivalent elastic modulus of the rib and costal cartilage components, the difference in chest circumference during respiration for the specific patient fell within the average range observed in the corresponding age and gender groups. Subsequently, the equivalent models were transformed into a realistic 3D model of the CWR implant, and FE analysis was conducted to evaluate the implant safety of the implant under conditions of chest compression, with a particular emphasis on the wavy-structured costal cartilage component. Implant designs demonstrating sufficient safety can be translated into models suitable for 3D printing. Nevertheless, A common dilemma lies in the difficulty of balancing flexibility and safety. The approach taken in this study was to choose the most flexible costal cartilage designs while ensuring that the maximum stress does not exceed the yield stress of the material. The wavy structure maintained several design parameters unchanged within a single costal cartilage component, potentially limiting safety improvements. For instance, the maximum stress in the wavy structure typically occurs at the peaks or troughs of the sinusoidal curve, where locally increasing the thickness and wave width could potentially reduce maximum stress while preserving flexibility, aiming for a more optimal balance between flexibility and safety.

This study presented a parametric design methodology for flexible CWR implants based on mechanical equivalent models, with PEEK as the subject material. Importantly, the proposed methodology in this research holds potential for application to other materials. On one hand, CWR implants made of any materials must adhere to three fundamental criteria: anatomical geometry, mechanical safety, and respiratory function. These criteria served as fundamental guiding principles throughout the design process, exhibiting their applicability across various implant materials. On the other hand, the methodologies employed in this study to determine the mechanical properties of rib and costal cartilage components, as well as to predict the respiratory function using equivalent mechanical properties as design parameters, can be extrapolated beyond PEEK and can be applied alternative materials, such as titanium alloys or polymers with lower elastic modulus.

An ongoing challenge in the clinical application of the methodology developed in this study was the complexity of constructing FE models for the natural chest wall. In conventional designs of PEEK CWR implants, the focus is primarily on reconstructing the bony structure of the rib cage and designing the geometry. This process could typically be accomplished within several hours. However, establishing a comprehensive FE model that encompasses the muscle-driven natural thorax with implants could be a time-consuming endeavour, requiring significant expertise from the design team. Therefore, a key area of future investigation revolves around simplifying the FE models of the chest wall, specifically tailored to simulate the respiratory function. Such efforts aim to gain a balance between model accuracy and computational efficiency. By simplifying and optimising the respiratory FE model, researchers will endeavour to facilitate the integration of the complex models into the clinical workflow, thereby enhancing their practicality and utility in clinics.

In addition to the three design criteria discussed in this study, a future design consideration for CWR implants that necessitates attention is the integration of the PEEK implant with both bone and soft tissues. Clinical follow-up has identified cases of implant exposure [46], which may be attributed to inadequate integration between the implant and soft tissue. Fixation of the CWR implant to the residual sternum or ribs using titanium wires or screws, while mechanically secure in short-term, may not be sufficient to withstand respiratory loads over extended periods of several decades [47,48]. To ensure long-term stability of the implant, a porous structure can be incorporated at the interface between

the implant and surrounding tissue to promote tissue ingrowth.

5. Conclusion

In this study, a design framework for flexible CWR implants is presented, which aims to address reduced respiration postoperatively while ensuring mechanical safety. The design framework relied on accurately predicting the deformation of the thoracic cage during respiration and understanding the relationship between the equivalent mechanical properties and the structural parameters of the rib and costal cartilage components of CWR implants. Quantitative control over the difference in chest circumference during respiration was achieved following the flexible CWR implantation, within a range of 50 mm to 63 mm. The effectiveness of the design framework was validated through numerical simulations based on a real clinical case, in which the flexible PEEK CWR implant increased the difference in chest circumference during respiration by 12.2 % compared to rigid PEEK implant, confirming its role in restoring respiratory function while ensuring the safety of the PEEK CWR implant.

Funding

CRediT authorship contribution statement

Changning Sun: Writing – original draft, Writing – review & editing, Visualization. **Enchun Dong:** Software, Visualization. **Yucong Tian:** Data curation, Methodology. **Jianfeng Kang:** Software. **Jibao Zheng:** Investigation, Methodology. **Qing Zhang:** Formal analysis, Validation. **Lei Wang:** Conceptualization, Resources. **Chaozong Liu:** Writing – review & editing, Formal analysis. **Ling Wang:** Formal analysis, Validation. **Dichen Li:** Conceptualization, Funding acquisition, Supervision.

Declaration of competing interest

The authors declare the following financial interests/personal relationships which may be considered as potential competing interests: Dichen Li reports financial support was provided by Xi'an Jiaotong University.

Data availability

Data will be made available on request.

Appendix A. Supplementary data

Supplementary data to this article can be found online at https://doi.org/10.1016/j.matdes.2023.112574.

References

[1] X.l. Ma, D.b. Wang, J.x. Ma, Y. Wang, L. Sun, B. Lu, Y. Wang, X.w. Zhao, F. Li, Z.r. Fan, Custom-made prosthesis for reconstruction after radical resection for chondrosarcoma of manubrium, Orthop. Surg. 10 (3) (2018) 272–275.

[2] L. Wang, X. Yan, J. Zhao, C. Chen, C. Chen, J. Chen, K.-N. Chen, T. Cao, M.-W. Chen, H. Duan, Expert consensus on resection of chest wall tumors and chest wall reconstruction, Transl. Lung Cancer Res. 10 (11) (2021) 4057.

[3] H. Huang, K. Kitano, K. Nagayama, J.-I. Nitadori, M. Anraku, T. Murakawa, J. Nakajima, Results of bony chest wall reconstruction with expanded polytetrafluoroethylene soft tissue patch, Ann. Thorac. Cardiovasc. Surg. 21 (2) (2015) 119–124.

[4] A. Turna, K. Kavakli, E. Sapmaz, H. Arslan, H. Caylak, H.S. Gokce, A. Demirkaya, Reconstruction with a patient-specific titanium implant after a wide anterior chest wall resection, Interact. Cardiovasc. Thorac. Surg. 18 (2) (2014) 234–236.

[5] J.L. Aranda, M.F. Jiménez, M. Rodríguez, G. Varela, Tridimensional titanium-printed custom-made prosthesis for sternocostal reconstruction, Eur. J. Cardiothorac. Surg. 48 (4) (2015) e92–e94.

[6] B. Yang, L. Zhou, J.-K. Chen, J. Wang, X.-P. Li, T. Jiang, Case Report Surgical planning by three dimensional printing for huge chondrosarcoma of chest wall resection, Int. J. Clin. Exp. Med. 9 (6) (2016) 12345–12347.

[7] I. Simal, M.A. García-Casillas, J.A. Cerdá, Ó. Riquelme, L. Lorca-García, L. Pérez-Egido, B. Fernández-Bautista, M. de la Torre, J.C. de Agustín, Three-dimensional custom-made titanium ribs for reconstruction of a large chest wall defect, Eur. J. Pediatr. Surg. Rep. 4 (01) (2016) 026–030.

[8] X. Wen, S. Gao, J. Feng, S. Li, R. Gao, G. Zhang, Chest-wall reconstruction with a customized titanium-alloy prosthesis fabricated by 3D printing and rapid prototyping, J. Cardiothorac. Surg. 13 (1) (2018) 4.

[9] L. Wang, T. Cao, X. Li, L. Huang, Three-dimensional printing titanium ribs for complex reconstruction after extensive posterolateral chest wall resection in lung cancer, J. Thorac. Cardiovasc. Surg. 152 (1) (2016) e5–e7.

[10] A.G. Alvarez, P.L. Evans, L. Dovgalski, I. Goldsmith, Design, additive manufacture and clinical application of a patient-specific titanium implant to anatomically reconstruct a large chest wall defect, Rapid Prototyp. J. 27 (2) (2021) 304–310.

[11] J.F. Kang, L. Wang, C.C. Yang, L. Wang, C. Yi, J. He, D. Li, Custom design and biomechanical analysis of 3D-printed PEEK rib prostheses, Biomech. Model. Mechanobiol. 17 (4) (2018) 1083–1092.

[12] L. Wang, C. Yang, C. Sun, X. Yan, J. He, C. Shi, C. Liu, D. Li, T. Jiang, L. Huang, Fused Deposition Modeling PEEK Implants for Personalized Surgical Application: From Clinical Need to Biofabrication, Int. J. Bioprinting 8 (4) (2022).

[13] I. Goldsmith, Chest Wall Reconstruction With 3D Printing: Anatomical and Functional Considerations, Innovations 17 (3) (2022) 191–200.

[14] J.S. Young, M. McAllister, M.B. Marshall, Three-dimensional technologies in chest wall resection and reconstruction, J. Surg. Oncol. 127 (2) (2023) 336–342.

[15] L. Wang, L. Huang, X. Li, D. Zhong, D. Li, T. Cao, S. Yang, X. Yan, J. Zhao, J. He, Y. Cao, L. Wang, Three-Dimensional Printing PEEK Implant: A Novel Choice for the Reconstruction of Chest Wall Defect, Ann. Thorac. Surg. 107 (3) (2019) 921–928.

[16] J. Aragón, I. Pérez Méndez, Dynamic 3D printed titanium copy prosthesis: a novel design for large chest wall resection and reconstruction, J. Thorac. Dis. 8 (6) (2016) E385–E389.

[17] J. Moradiellos, S. Amor, M. Córdoba, G. Rocco, M. Vidal, A. Varela, Functional Chest Wall Reconstruction With a Biomechanical Three-Dimensionally Printed Implant, Ann. Thorac. Surg. 103 (4) (2017) e389.

[18] M.P. Fiorucci, A. Cuadrado, A. Yánez, O. Martel, B. Mentado, D. Monopoli, Biomechanical characterization of custom-made dynamic implants fabricated by Electron Beam Melting for anterior chest wall reconstruction, Mater. Des. 206 (2021), 109758.

[19] C.N. Sun, L. Wang, J.F. Kang, D.C. Li, Z.M. Jin, Biomechanical Optimization of Elastic Modulus Distribution in Porous Femoral Stem for Artificial Hip Joints, J. Bionic Eng. 15 (4) (2018) 693–702.

[20] C. Sun, E. Dong, J. Chen, J. Zheng, J. Kang, Z. Jin, C. Liu, L. Wang, D. Li, The Promotion of Mechanical Properties by Bone Ingrowth in Additive-Manufactured Titanium Scaffolds, J. Funct. Biomater. 13 (3) (2022).

[21] J.L. Forman, E.D.P. De Dios, R.W. Kent, A pseudo-elastic effective material property representation of the costal cartilage for use in finite element models of the whole human body, Traffic Injury Prev. 11 (6) (2010) 613–622.

[22] C. Zhang, L. Wang, J. Kang, O.M. Fuentes, D. Li, Bionic design and verification of 3D printed PEEK costal cartilage prosthesis, J. Mech. Behav. Biomed. Mater. 103 (2020), 103561.

[23] J. Kang, Y. Tian, J. Zheng, D. Lu, K. Cai, L. Wang, D. Li, Functional design and biomechanical evaluation of 3D printing PEEK flexible implant for chest wall reconstruction, Comput. Methods Programs Biomed. 225 (2022), 107105.

[24] E. Soleyman, M. Aberoumand, K. Soltanmohammadi, D. Rahmatabadi, I. Ghasemi, M. Baniassadi, K. Abrinia, M. Baghani, 4D printing of PET-G via FDM including tailormade excess third shape, Manuf. Lett. 33 (2022) 1–4.

[25] D. Rahmatabadi, I. Ghasemi, M. Baniassadi, K. Abrinia, M. Baghani, 4D printing of PLA-TPU blends: effect of PLA concentration, loading mode, and programming temperature on the shape memory effect, JMatS 58 (16) (2023) 7227–7243.

[26] E. Soleyman, D. Rahmatabadi, K. Soltanmohammadi, M. Aberoumand, I. Ghasemi, K. Abrinia, M. Baniassadi, K. Wang, M. Baghani, Shape memory performance of PETG 4D printed parts under compression in cold, warm, and hot programming, Smart Mater. Struct. 31 (8) (2022).

[27] A. Ratnovsky, D. Elad, Anatomical model of the human trunk for analysis of respiratory muscles mechanics, Respir. Physiol. Neurobiol. 148 (3) (2005) 245–262.

[28] M. Behr, J. Pérès, M. Llari, Y. Godio, Y. Jammes, C. Brunet, A three-dimensional human trunk model for the analysis of respiratory mechanics, (2010).

[29] M. Christophy, N.A. Faruk Senan, J.C. Lotz, O.M. O'Reilly, A musculoskeletal model for the lumbar spine, Biomech. Model. Mechanobiol. 11 (2012) 19–34.

[30] F.H. Cheng, S.L. Shih, W.K. Chou, C.L. Liu, W.H. Sung, C.S. Chen, Finite element analysis of the scoliotic spine under different loading conditions, Biomed. Mater. Eng. 20 (5) (2010) 251–259.

[31] H. Ladjal, B. Shariat, J. Azencot, M. Beuve, Appropriate biomechanics and kinematics modeling of the respiratory system, in: Human Diaphragm and Thorax,

2013 IEEE/RSJ International Conference on Intelligent Robots and Systems, 2013, pp. 2004–2009.

[32] H. Ladjal, N. Skendraoui, M. Giroux, Y. Touileb, J. Azencot, B. Shariat, H. Ladjal, M. Beuve, P. Giraud, Physiological and biomechanical model of patient specific lung motion based on 4D CT images, in: 2015 8th Biomedical Engineering International Conference (BMEiCON), 2015, pp. 1–5.

[33] B.Y. Guo, D.H. Liao, X.Y. Li, Y.J. Zeng, Q.H. Yang, Age and gender related changes in biomechanical properties of healthy human costal cartilage, Clin. Biomech. (Bristol, Avon) 22 (3) (2007) 292–297.

[34] K. Shigeta, Y. Kitagawa, T. Yasuki, Development of next Generation Human Fe Model Capable of Organ Injury Prediction (2009).

[35] H. Ladjal, J. Azencot, M. Beuve, P. Giraud, J.M. Moreau, B. Shariat, Biomechanical Modeling of the Respiratory System: Human Diaphragm and Thorax, in: B. Doyle, K. Miller, A. Wittek, P.M.F. Nielsen (Eds.), Computational Biomechanics for Medicine, Springer International Publishing, Cham, 2015, pp. 101–115.

[36] M.P. Pato, N.J. Santos, P. Areias, E.B. Pires, M. de Carvalho, S. Pinto, D.S. Lopes, Finite element studies of the mechanical behaviour of the diaphragm in normal and pathological cases, Comput. Methods Biomech. Biomed. Eng. 14 (6) (2011) 505–513.

[37] M. Behr, L. Thollon, P.-J. Arnoux, T. Serre, S.V. Berdah, P. Baque, C. Brunet, 3D reconstruction of the diaphragm for virtual traumatology, Surg. Radiol. Anat. 28 (3) (2006) 235–240.

[38] J. Zheng, J. Kang, C. Sun, C. Yang, L. Wang, D. Li, Effects of printing path and material components on mechanical properties of 3D-printed polyether-ether-ketone/hydroxyapatite composites, J. Mech. Behav. Biomed. Mater. 118 (2021), 104475.

[39] G. Zhang, X. Chen, J. Ohgi, T. Miura, A. Nakamoto, C. Matsumura, S. Sugiura, T. Hisada, Biomechanical simulation of thorax deformation using finite element approach, Biomed. Eng. Online 15 (1) (2016) 1–18.

[40] K.G. Gruben, A.D. Guerci, H.R. Halperin, A.S. Popel, J.E. Tsitlik, Sternal Force-Displacement Relationship During Cardiopulmonary Resuscitation, J. Biomech. Eng. 115 (2) (1993) 195–201.

[41] T.A. Wilson, A. Legrand, P.-A. Gevenois, A. De Troyer, Respiratory effects of the external and internal intercostal muscles in humans, J. Physiol. 530 (2) (2001) 319–330.

[42] G. Zhang, X. Chen, J. Ohgi, T. Miura, A. Nakamoto, C. Matsumura, S. Sugiura, T. Hisada, Biomechanical simulation of thorax deformation using finite element approach, Biomed. Eng. Online 15 (1) (2016) 18.

[43] S.A. Naghavi, C. Sun, M. Hejazi, M. Tamaddon, J. Zheng, L. Wang, C. Zhang, S. N. Varma, D. Li, M. Moazen, L. Wang, C. Liu, On the mechanical aspect of additive manufactured polyether-ether-ketone scaffold for repair of large bone defects, Biomater. Transl. 3 (2) (2022) 142–151.

[44] G.N. Rutty, C. Robinson, J. Amoroso, T. Coats, B. Morgan, Could post-mortem computed tomography angiography inform cardiopulmonary resuscitation research? Resuscitation 121 (2017) 34–40.

[45] S. Changning, K. Jianfeng, Y. Chuncheng, Z. Jibao, S. Yanwen, D. Enchun, L. Yingjie, Y. Siqi, S. Changquan, P. Huanhao, H. Jiankang, W. Ling, L. Chaozong, P. Jianhua, L. Liang, J. Yong, L. Dichen, Additive manufactured polyether-ether-ketone implants for orthopaedic applications: a narrative review, Biomater. Transl. 3 (2) (2022) 00.

[46] C. Sun, H. Zhao, L. Wang, J. Zhang, J. Zheng, Z. Yang, L. Huang, L. Wang, C. Liu, D. Li, Q. Li, Additive manufactured polyether-ether-ketone composite scaffolds with hydroxyapatite filler and porous structure promoted the integration with soft tissue, Biomater. Adv. 141 (2022), 213119.

[47] J. Zheng, H. Zhao, E. Dong, J. Kang, C. Liu, C. Sun, D. Li, L. Wang, Additively-manufactured PEEK/HA porous scaffolds with highly-controllable mechanical properties and excellent biocompatibility, Mater. Sci. Eng. C 128 (2021), 112333.

[48] J. Zheng, H. Zhao, Z. Ouyang, X. Zhou, J. Kang, C. Yang, C. Sun, M. Xiong, M. Fu, D. Jin, L. Wang, D. Li, Q. Li, Additively-manufactured PEEK/HA porous scaffolds with excellent osteogenesis for bone tissue repairing, Compos. B Eng. 232 (2022), 109508.